

Reconfigurable Metasurfaces for Frequency Selective Absorption

Heijun Jeong, Dinh Hai Le, Daecheon Lim, Ratanak Phon, and Sungjoon Lim*

Metasurfaces can provide novel functionality for absorbing electromagnetic waves through a periodic array of inductive/capacitive resonators by controlling the material's permittivity and permeability. This attractive characteristic makes them widely applicable to various electromagnetic applications. However, conventional metasurfaces are dispersive and suffer from a narrow bandwidth with uncontrollable and unchangeable functions because the effective permittivity and permeability are tailored to a certain resonance frequency. Therefore, many studies have focused on how to increase the absorption frequency bandwidth and control the absorption frequency by using reconfigurable metasurfaces. This paper presents a report on the most recent progress in the realization of reconfigurable metasurfaces based on advanced materials for frequency-selective absorption in the microwave, millimeter-wave, sub-terahertz, terahertz, and visible ranges. Furthermore, their tuning ratios for different advanced materials and spectra are summarized and compared. This progress report provides guidelines for the material selection for and the design of reconfigurable metasurfaces.

1. Introduction

Metamaterials (MMs) are artificial sub-wavelength-thickness structures consisting of infinitely arranged periodic unit cells (e.g., “meta-atoms”).^[1] The building blocks of metasurfaces (MSs) are 2D arrays of engineered meta-atoms resembling MMs that utilize light–matter interactions for specific purposes. They have been used in many electromagnetic applications, such as artificial magnetic conductors,^[2–4] electromagnetic bandgap surfaces,^[5,6] high impedance surfaces,^[7] frequency-selective surfaces,^[8,9] scattering,^[10] and superstrates.^[11,12]

Especially, metasurface absorbers (MSAs) are promising structures for use in health, energy, electronics, and defense applications.^[13–15] In the past decade, material-based absorbers such as ferrite or composite absorbers have been commonly used as electromagnetic absorbers.^[16–21] In spite of the high absorptivity and wide absorption bandwidth of the absorbing materials, they are complicated, expensive, and bulky, which are critical drawbacks for defense applications such as stealth


technology, and structure-based absorbers such as Jaumann or Salisbury screen absorbers have been proposed to overcome these.^[22,23] However, they remain relatively bulky and their physical thickness increases as the resonance frequency decreases because of the quarter-wave ($\lambda/4$) length in the design. In 2008, Landy et al.^[14] first proposed an MSA with high absorptivity and a low profile; the high absorptivity was achieved by tailoring the effective permittivity and permeability. Because an MSA consists of a periodic array of a metallic pattern on a dielectric material, this offers a simple and cost-effective fabrication process. MSAs with symmetric unit cells that maintain high absorptivity at all polarization angles have been fabricated.^[24,25] Because MSAs are anisotropic, their absorptivity is degraded at wide incidence angles, and MSAs with angle-insensitive or subwavelength unit

cells have been proposed to overcome this incidence angle sensitivity.^[26,27]

MSAs inherently show narrow frequency bandwidth because of the resonance characteristic, which is useful for energy, imaging, and sensor applications requiring high-frequency selectivity.^[28–30] However, this can be disadvantageous for radar cross-section (RCS) and electromagnetic-interference reduction requiring broadband coverage. Dual-band and multi-band MSAs that can overcome the narrow bandwidth of MSAs by generating multiresonance have been recommended.^[31,32] Moreover, broadband MSAs using resistive patterns, resistor elements, lossy materials, and multilayers have been suggested.^[15,33–35] Alternatively, diffusion MSs have been proposed for broadband RCS reduction.^[36–39] A diffusion MS generates different phase distributions and scattering patterns. Thus, it can reduce RCS by scattering incident electromagnetic waves rather than absorbing them. A broadband diffusion MS is thinner than a broadband MSA, but there is still the possibility of detection by multistatic radar. Nevertheless, scattering is traditionally an effective method for RCS reduction.

Compared to material-based absorbers, one of the advantages of MSAs is reconfigurability and functionality. An MSA can be integrated with tunable components and various advanced materials. In addition, a reconfigurable MSA can overcome the narrow bandwidth problem,^[34,40,41] respond to diverse electromagnetic scenarios, and switch its function. Its frequency reconfigurability can also be used for sensor and imaging applications.^[28–30]

H. Jeong, D. H. Le, D. Lim, R. Phon, Prof. S. Lim
School of Electrical and Electronic Engineering
Chung-Ang University
221 Heukseok-Dong, Dongjak-Gu, Seoul 06974, Republic of Korea
E-mail: sungjoon@cau.ac.kr

 The ORCID identification number(s) for the author(s) of this article can be found under <https://doi.org/10.1002/adom.201902182>.

DOI: 10.1002/adom.201902182

Because early MSAs were mostly studied in the microwave region, they were applied for RCS reduction to improve stealth.^[27,34,35,42] Later, advances in nanotechnologies paved the way for terahertz (THz) and infrared MSAs.^[29,30,43] Therefore, they have been diversely applied in the fields of imaging, energy, and sensors. On the other hand, their operational frequency has been lowered to a few MHz and kHz due to the high demand for acoustic and electromagnetic-interference absorbers.^[44–46] Millimeter-wave and sub-THz MSAs are expected to play an important role in 5G and 6G wireless communication.^[47–49] A growing trend toward more functionality and adaptive response of MSAs has brought about reconfigurable MSAs. Because the performances of these are dependent on tunable materials, various advanced materials have been used in reconfigurable MSAs and material selection is also dependent on the frequency.

Herein, we briefly report the advanced material-based reconfigurable metasurfaces for frequency-selective absorption in the microwave, millimeter-wave, sub-THz, THz, and visible regions. We discuss the specific advanced materials that are generally applied to active MM absorbers for each frequency region. First, we explain the electronic tuning mechanisms in the microwave region using PIN and varactor diodes, fluidic tuning using distilled water and liquid metal, and thermal tuning using germanium telluride (GeTe) and strontium titanate (STO). We then discuss liquid crystal and optical tuning mechanisms in the millimeter-wave and sub-THz bands using photoexcitation and THz pulses. In the next section, we discuss liquid crystal, graphene, microelectromechanical systems (MEMS), and vanadium dioxide (VO₂) materials for reconfigurable MSAs in the THz band. Finally, we conclude this progress report with a systematic summary and give a brief comparison of advanced material-based reconfigurable MSA performances.

2. Reconfigurable MSAs in the Microwave Region

The microwave region typically refers to frequencies from 300 MHz to 30 GHz and has been widely studied with respect to wireless communication. It is commonly divided into the L (1–2 GHz), S (2–4 GHz), C (4–8 GHz), X (8–12 GHz), Ku (12–18 GHz), and K (18–26.5 GHz) bands, with various primary uses. MSAs have been studied extensively for operating in the microwave region. Since the X-band is commonly used for radar, many MSAs have been investigated to avoid radar detection. One well-known method of adding active features for operating in the microwave region is to add elements to a circuit using PIN or varactor diodes, thereby modifying the resonance frequency by changing the MSA capacitance or inductance. Alternatively, many studies have considered active features using microfluidic channels for the microwave bands. Injecting liquid through microfluidic channels can significantly alter the substrate characteristics and eliminate additional bias circuitry.

2.1. Electronic Tuning

Active microwave range MM absorbers containing PIN and varactor diodes have been extensively employed in antennas



University, Seoul, South Korea. His research interests are functional metasurfaces and 3D printed metasurfaces.

Heijun Jeong received a B.S. degree in information and communication engineering from An-Yang University, Gyeonggi, South Korea, in 2016, and M.S. degree in electrical and electronics engineering from Chung-Ang University, Seoul, South Korea, in 2018. He is currently pursuing a Ph.D. degree in electrical and electronics engineering at Chung-Ang



Dinh Hai Le received a B.S. degree from the Physics Department at Hanoi National University of Education, Hanoi, Vietnam, in 2016. Since 2018, he is currently pursuing an M.S. degree in electrical and electronics engineering at Chung-Ang University, Seoul, South Korea. His research interests are reconfigurable metasurfaces and origami/kirigami-inspired metasurfaces.



Korea, in 2007, where he is currently a full Professor. His research interests include engineered electromagnetic structures (metamaterials and metasurfaces).

Sungjoon Lim received M.S. and Ph.D. degrees in electrical engineering from the University of California in Los Angeles, USA, in 2004 and 2006, respectively. After a postdoctoral position at the Integrated Nanosystem Research Facility, University of California, Irvine, USA, he joined the School of Electrical and Electronics Engineering, Chung-Ang University, Seoul,

and circuits in conventional microwave applications. To realize electronic tuning in the microwave region, PIN and varactor diodes are most commonly used to achieve frequency reconfigurable MSAs.^[50–57] The PIN diode behaves like a device in series with resistance and inductance when in the ON state. On the other hand, when the PIN diode is in the OFF state, it is working at low capacitance and inductance.

As a result, the PIN diode works as a short/open circuit by switching between the ON/OFF states and in general, is placed between the conductive patterns in the MSA unit cell. Therefore, the frequency switching capability can be achieved by changing the electrical length of the unit cell depending on the ON/OFF state. A typical frequency switchable MSA from high frequency to low frequency by turning ON the PIN diode. For instance, a single-band switchable MSA with two identical split-ring resonators is shown in **Figure 1a**.^[58] Because a single PIN diode is connected between two resonators, the absorption frequency is switched from 2.55 to 2.95 GHz by turning it ON. Figure 1b shows a dual-band switchable MSA using PIN diodes on an annular ring and cross-dipole: four PIN diodes are placed on

the annular ring and the other four are placed on the cross-dipole. Therefore, the dual-band frequency is independently switched from 2.00 to 3.68 GHz and 4.02 to 6.37 GHz. Similarly, a single-band MSA can be switched to a dual-band MSA, as shown in Figure 1c.^[51] The outer square loop has four PIN diodes and the inner cross has four PIN diodes, thus the four different switching combinations in the MSA produce two single-band states (3.52 and 8.85 GHz) and two dual-band states (3.52/8.85 and 7.7/8.91 GHz).

Figure 1d shows a broadband-switchable MSA using PIN diodes.^[55] The broadband-frequency bandwidth is achieved by loading the lumped resistors on the top conductive pattern. The switchable frequency is achieved using the switchable ground plane, which is built between the top and bottom planes.

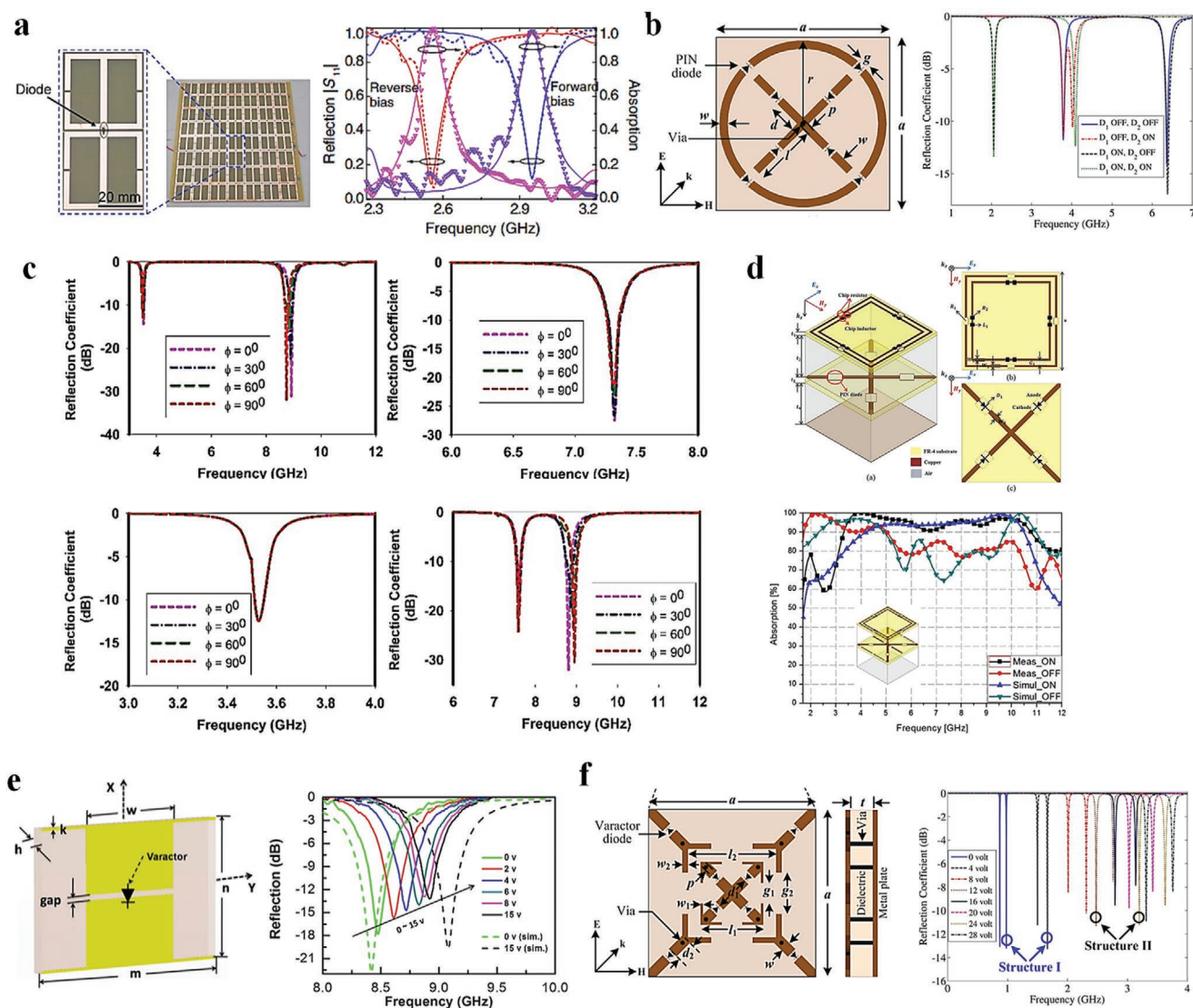


Figure 1. Microwave reconfigurable metasurface absorbers (MSAs) using electrical tuning methods. The geometry and absorption ratio using PIN diodes: a) a single-frequency switching MSA, b) a dual-frequency switching MSA, c) a single-to-dual-band switchable MSA, and d) a broadband-frequency switchable MSA. The geometry and absorption ratio using varactor diodes: e) a single-frequency reconfigurable MSA and f) a multi-frequency reconfigurable MSA. a) Reproduced with permission.^[58] Copyright 2010, EMW Publishing. b) Reproduced with permission.^[112] Copyright 2017, IEEE. c) Reproduced with permission.^[51] Copyright 2017, IEEE. d) Reproduced with permission.^[55] Copyright 2019, Springer Nature Publishing AG. e) Reproduced with permission.^[50] Copyright 2018, AIP Publishing LLC. f) Reproduced with permission.^[53] Copyright 2017, IEEE.

When the PIN diode is ON, the broadband MSA is realized at high frequency (3.5–11 GHz) because the switchable ground plane is working as the ground plane whereas when the PIN diode is OFF, the broadband MSA is realized at low frequency (1.7–5.2 GHz) because the switchable ground plane is working as the reactance plane.

On the other hand, a reconfigurable continuous-frequency MSA can be achieved by using the varactor diode because its capacitance is continuously varied by changing the voltage. In general, the varactor diode is placed on the small gap between the conductive patterns of a unit cell. Figure 1e shows a typical reconfigurable continuous-frequency MSA using the varactor diode where a single narrow absorption band is continuously changed.^[50] Higher absorption frequency is achieved by lowering the capacitance of the varactor diode; for instance, when the applied voltage is increased from 0 to 15 V, the absorption frequency is decreased from 9.1 to 8.4 GHz. Although the frequency-tuning ratio of the MSA is highly dependent on the variable capacitance range of the varactor diode, it can be enhanced by loading the varactor diode on the gap generating the strongest electric response. Figure 1f shows a reconfigurable dual-band frequency MSA with the varactor diode.^[53] It consists of two single-band tunable structures: one resonates in the L-band while the other resonates in the S-band. Because each resonator has four varactor diodes, the dual band of the MSA can be independently changed from 0.98 to 3.81 GHz and from 0.91 to 3.3 GHz. Although PIN diodes are widely used in broadband-switchable MSAs, varactor diodes are not because the tuning effect is limited in the broadband spectrum. Nevertheless, the continuous tuning capability of the varactor diode should be advantageous for a reconfigurable MSA.

Recently, a frequency reconfigurable MSA using a combination of varactor and PIN diodes has been proposed.^[52] It consists of two structured layers where the top layer has an I-shaped pattern with a single varactor diode and the middle layer has a split wire with a single PIN diode. Its absorption frequency can be changed from 2.9 to 3.7 GHz by varying the capacitance of the varactor diode. In addition, its absorptivity can be changed from 60% to 97% by varying the resistance of the PIN diode. Instead of the ON/OFF switching operation, the PIN diode is used as a variable resistor. The absorption mode of the switchable MSA can be switched to reflection mode by using the PIN diode.^[56] It is designed with inner square loops, each of which is connected to four outer square loops through PIN diodes. Therefore, the MSA can be dramatically switched to high impedance, resulting in reflectance.

In conclusion for this section, we introduced electrically reconfigurable frequency MSAs operating in the microwave region and mentioned that PIN and varactor diodes are commonly used for electric tuning. These materials can be used to tune the frequency immediately and offer great tunability for MSAs. However, some challenging research still remains to be conducted, such as bias networks or complex designs due to scattering and/or degraded performance. In addition, this approach is limited to higher frequencies such as in the THz region because of parasitic resistance and reactance.

2.2. Fluidic Tuning Mechanisms

Fluidic tuning technology can also provide excellent MSAs in the microwave region that do not require electronic devices, additional DC bias, or complex fabrication processes. Therefore, fluidic tuning technology is an attractive research topic for active MSAs to overcome the main drawbacks of electrically tuned MSAs. However, their low tuning speed and the requirement for very highly precise injection channel dimensions are their main disadvantages. Many fluidics have been proposed for active MSAs, such as distilled water, oil, ethanol, and liquid metal. In this section, we discuss active MM absorbers using distilled water and liquid metals, which are commonly used as active MSAs.

Distilled water is an attractive material for a fluidic tuning because it can solve MSA narrow bandwidth problems. Storing distilled water in the substrate and placing the metallic plane back from the substrate causes the distilled water to become a broadband MSA because it has a large imaginary permittivity component and is frequency dispersive.^[59–65] Thus, broadband MSAs can be realized using an all-dielectric MSA and injecting distilled water as shown in Figure 2a.^[66] After optimization, the system achieved >90% absorption for 6.4–30 GHz, with a good match between the simulation and measurement results (Figure 2b). Injected distilled water can also act as a multifunctional MSA. Zhao and Zhou^[67] proposed a tunable MSA with switchable absorption and transmission by injecting water or not, respectively, as shown in Figure 2d,e. Without injecting distilled water, the proposed MSA operated as a transmitter at 10.6, 15.5, and 16.8 GHz with corresponding 0.67, 0.52 dB, and 2.5 dB insertion losses. With injecting distilled water, the proposed MM operated as an all-dielectric broadband MSA, achieving 90% absorption at 10–20 GHz.

The switchable characteristic of liquid metals makes them attractive for active MSAs. Recent MSA studies have constructed frequency switchable MSAs by injecting liquid metal into fluid channels, thereby changing the MSA capacitance or inductance and thus causing frequency switching.^[68–71] MSAs can have flexible characteristics because liquid metal can also be exploited in a flexible substrate. For example, Kim et al.^[69] proposed a wideband-switchable MSA using injected liquid metal to increase its capacitance due to the capacitance difference between the top conductive patterns and the injected liquid metal. Figure 3a shows their flexible MSA using injected liquid metal. When liquid metal was not injected, the MSA exhibited 90% absorption at 7.43–14.34 GHz whereas 90% absorption was achieved at 5.62–7.3 GHz when liquid metal was injected (Figure 3b), thus confirming frequency switching by injecting liquid metal into the channels.

One drawback when creating active MSAs by injecting liquid metal is that they become polarization-sensitive because the fluid channels create rows. Therefore, Lim et al.^[70] proposed a polarization-insensitive frequency switchable MSA using liquid metal. Figure 3c shows their design involving two opposite direction fluidic channels in the middle of a substrate. The proposed MSA was polarization-insensitive due to the symmetrical structure and could switch absorption frequencies to achieve a 90% absorption bandwidth at 2.48–8.1 GHz without liquid metal injection and a 90% absorption bandwidth at

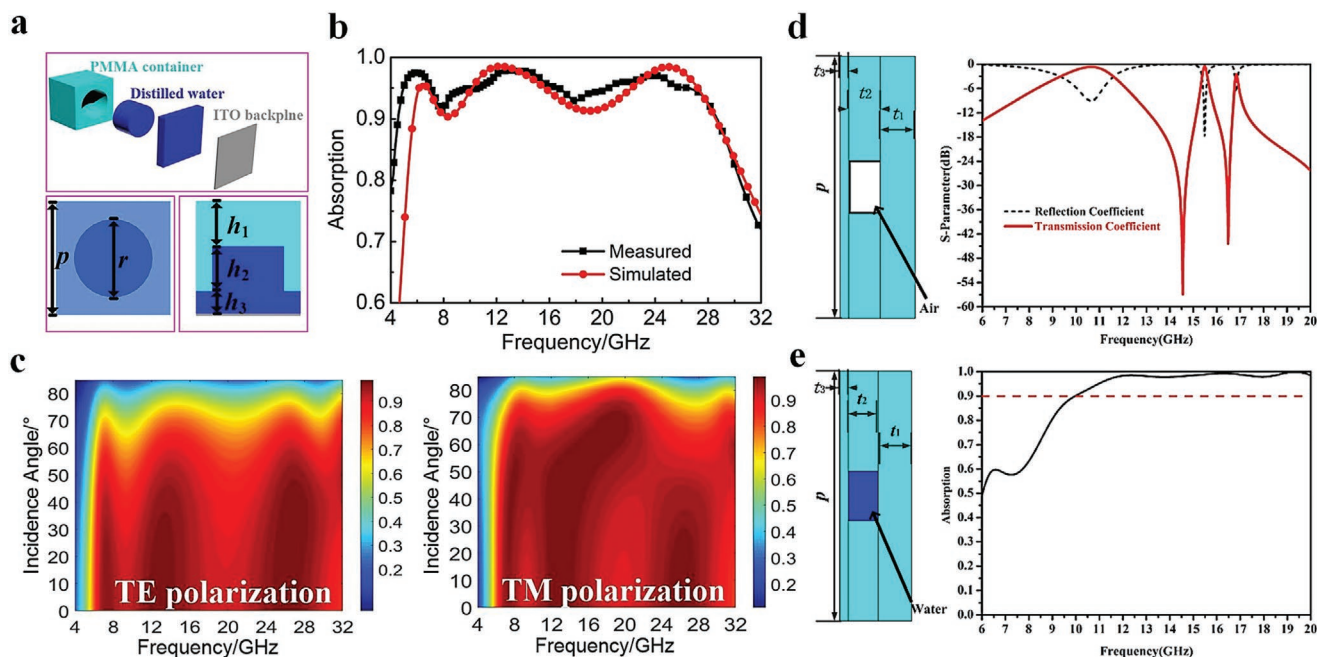


Figure 2. Fluidic reconfigurable metasurface absorbers (MSAs) using distilled water: a) the geometry, b) simulated and measured absorption, c) measured absorption with respect to the oblique incidence angle of a multifunctional MSA by injecting distilled water, d) design and S-parameters without injected water, and e) design and absorption with injected water. a-c) Reproduced with permission.^[66] Copyright 2018, AIP Publishing LLC. d,e) Reproduced with permission.^[67] Copyright 2018, IEEE.

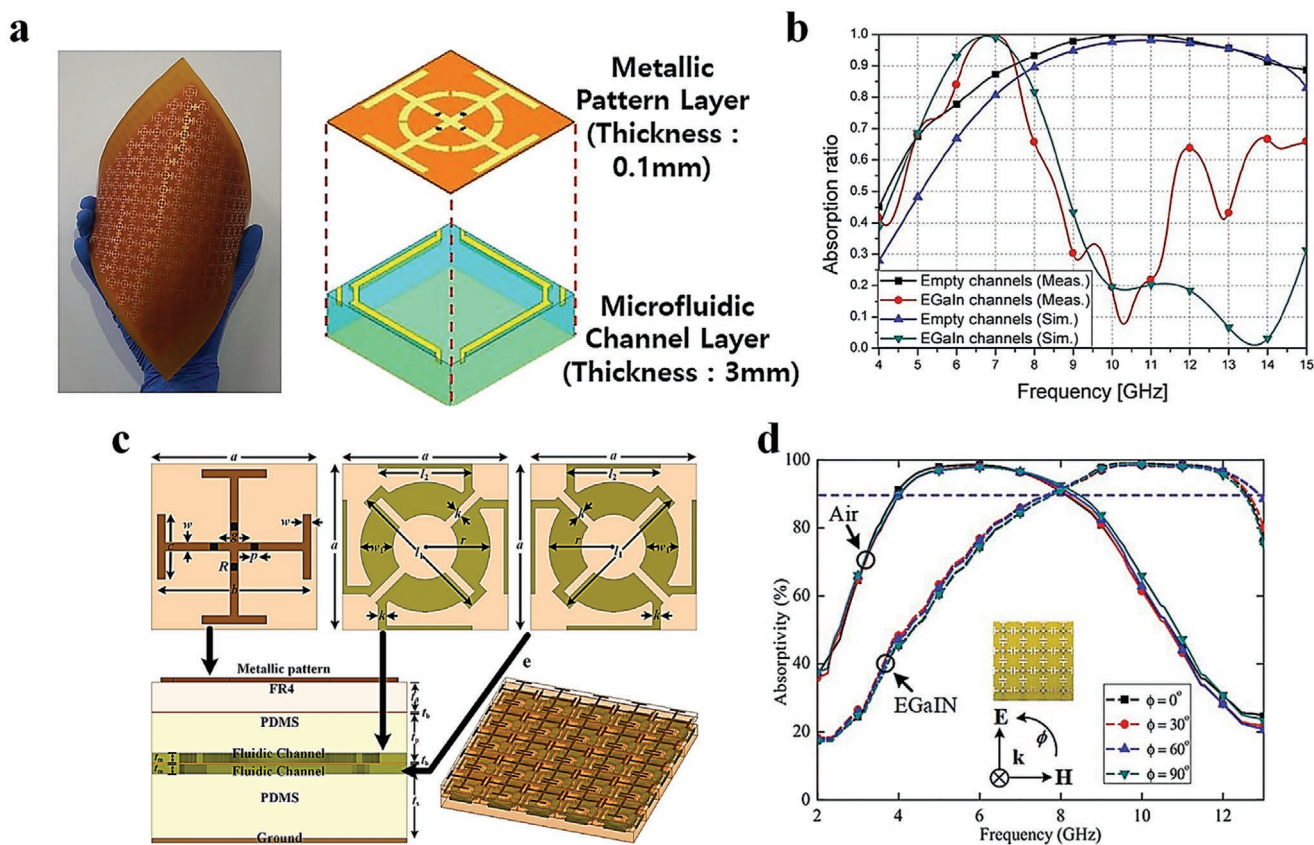


Figure 3. Frequency switchable metasurface absorbers (MSAs) using liquid metal: a) the geometry and b) simulated and measured absorption, c) the geometry of a polarization-insensitive frequency switchable MSA using liquid metal, and d) the measured absorption with and without injected liquid metal. a,b) Reproduced with permission.^[69] Copyright 2016, Springer Nature Publishing AG. c,d) Reproduced with permission.^[70] Copyright 2018, Springer Nature Publishing AG.

7.98–12.24 GHz with liquid metal injection (Figure 3d), with the absorption range and efficacy remaining unchanged with respect to the polarization angle.

2.3. Thermal Tuning Mechanisms

Thermal materials can also be used as active MSAs in the microwave region. As discussed previously, electrically active MSAs require additional direct current (DC) bias circuitry to operate the electrical components and fluidic-active MM absorbers have a slow tuning speed. These drawbacks can be addressed using thermally tunable materials. For example, germanium telluride (GeTe) can thermally switch between amorphous (high-resistive or insulating) and crystalline (low-resistive or conductive) states. Moreover, a power system is not required since varying the temperature can be used to switch between these states. Jeong et al.^[72] proposed a thermally active MSA using a GeTe material. They designed a circular unit cell with a gap on either side in which they placed GeTe to maximize the switching frequency range, as shown in Figure 4a. They characterized GeTe conductivity in its amorphous and crystalline states by measuring the deposited GeTe sheet resistance at room temperature and 250 °C (0.63×10^{-2} and 3.2×10^5 s m⁻¹, respectively). Figure 4c shows that the absorption frequency switched from 10.23 to 9.6 GHz when the GeTe state was changed from amorphous (room temperature) to crystalline (250 °C), with corresponding absorptivity values of 91% and 92%, respectively.

Strontium titanate (STO) is another excellent candidate for thermally active MSAs.^[73] STO is a ferroelectric material with high permittivity and low dielectric loss, and also

changes permittivity with temperature. STO permittivity can be calculated as

$$\varepsilon(k) = \varepsilon_{\infty} + \frac{F}{k_0^2 - k^2 - ik\gamma} \quad (1)$$

$$k_0(T)[\text{cm}^{-1}] = \sqrt{31.2(T - 42.5)} \quad (2)$$

and

$$\gamma[\text{cm}^{-1}] = -3.3 + 0.049T \quad (3)$$

where k is the incident wave number, $\varepsilon_{\infty} = 9.6$ is the limited permittivity, F is the resonance strength, γ is the damping constant, and k_0 is the soft mode wave number. Thus, the permittivity of STO depends on the external temperature. Wang et al.^[73] designed a thermally frequency-tunable MSA using STO with an electric resonance ring (ERR) by placing the STO near the ERR structure, as shown in Figure 4d. Figure 4e shows that STO permittivity decreases as temperature decreases. Thus, they realized a frequency-tunable MSA according to STO temperature, as shown in Figure 4f.

In this section, we discussed tunable MSAs within the microwave region where the most commonly used methods are diodes or microfluidic channels, which are also used in other RF devices. Current studies have shown excellent MSA performance across the microwave region, but a limit is met in the higher frequency bands. Diodes have maximum usable frequency only in the microwave region. Although some diodes can be fabricated for higher frequency bands, the cost becomes onerous.

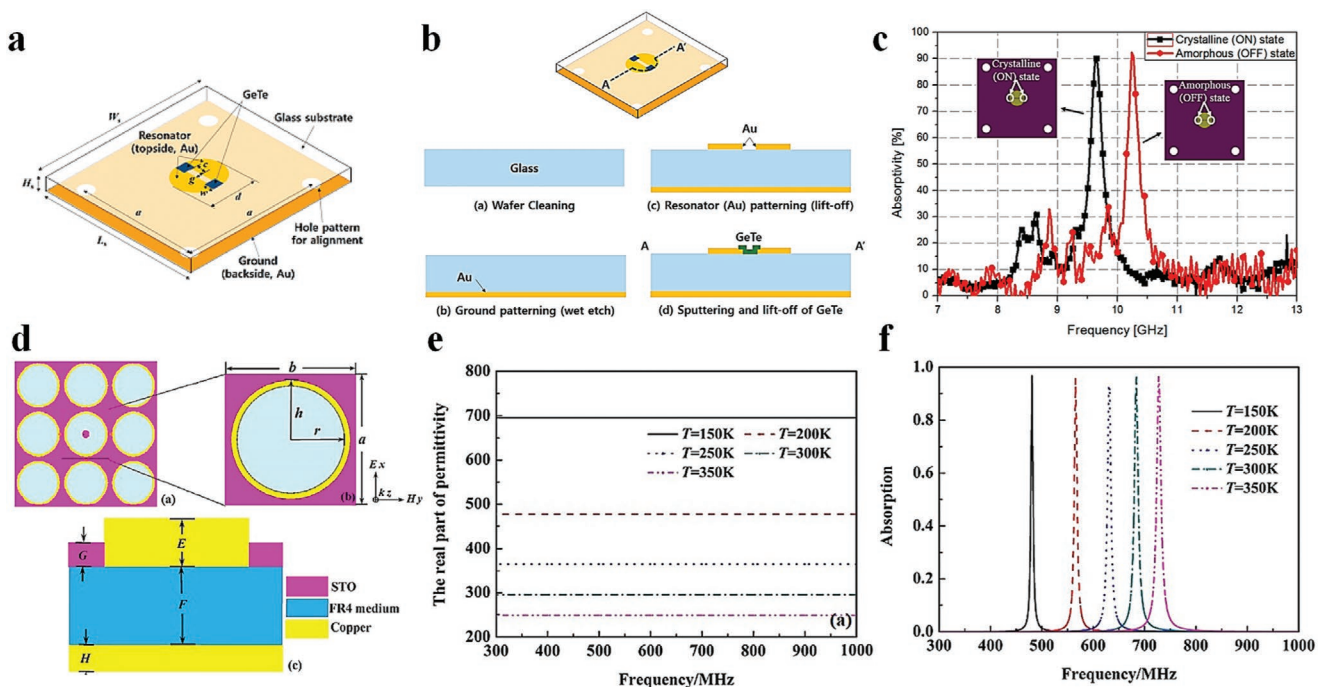


Figure 4. Thermally reconfigurable metasurface absorbers (MSAs) using advanced materials. GeTe-based active MSAs: a) the 3D unit cell geometry, b) fabrication process, and c) measured absorptivity for different GeTe states. Strontium titanate-based active MSAs: d) the geometry, e) STP permittivity with respect to temperature, and f) MSA absorptivity with respect to temperature. a–c) Reproduced with permission.^[72] Copyright 2018, MDPI. d–f) Reproduced with permission.^[73] Copyright 2019, Informa UK Limited.

Designing microfluidic-channel devices for high-frequency bands is somewhat difficult because the channels can be very small. Thermal tuning also provides excellent active MSA candidates for the microwave region because these do not require additional DC bias and have high tuning speed. However, they are also difficult to design to achieve the specifically desired frequency. These drawbacks mean that the methods introduced in this section are mainly used for the microwave region, with other methods being employed to design active MSAs in other frequency regions.

3. Reconfigurable MSAs in the Millimeter-Wave and Sub-THz Regions

Millimeter-wave (30–300 GHz, 1–10 mm) and sub-THz (0.1–1 THz, 0.3–3 mm) radiation are located between the THz and microwave regions, and thus share some properties with the THz and microwave ranges. Millimeter-wave and sub-THz technologies have experienced rapid development over the last few years with essential applications in energy,^[74] medicine,^[75] environmental science,^[76] and electrical engineering.^[77,78] They also have vital roles in fifth-generation (5G) wireless broadband communication due to the enormous amount of available bandwidth in this frequency range.^[79] Therefore, millimeter-wave and sub-THz MMs and particularly MSAs have received significant research attention.

Millimeter-wave and sub-THz absorbers provide important electromagnetic protection and have been widely investigated and employed to dissipate jamming signals, thereby greatly improving the overall system performance.^[80] Although these bands have

several major drawbacks, including low light transmission and difficult fabrication, many narrowband,^[81] broadband,^[80,82] polarization, and wide-incident-angle-insensitive absorbers have been reported.^[83–85] However, most are passive absorbers with fixed operating frequencies, which restricts their applications. As discussed in the introduction, active or functional MMs and MSAs have a wide range of applications in modern integrated systems and multifunctional devices. However, the resonator size in these ranges, particularly for sub-THz, is microscale and so microfluidic, PIN diode, varactor diode, or other chip elements face significant fabrication and measurement challenges. The two main techniques to achieving active millimeter-wave and sub-THz band MSAs are liquid crystals (LCs) and optical tuning.

3.1. LC Tuning

Materials in LC states simultaneously exhibit conventional liquid and solid crystal properties and are thus promising candidates for active MSAs due to their cost-effectiveness, ease of manufacture, and birefringence.^[86,87] Importantly, LC orientation can be externally controlled by varying the temperature, incident light, and electromagnetic fields, thereby creating active LC-integrated devices. Spectral shifting by changing the LC orientation leads to anisotropic permittivity modulation and consequently, resonance or absorption switching. For example, Yin et al.^[88] reported an LC-based electrically tunable dual-band MSA for the millimeter-wave range. **Figures 5a** and **6b** show the proposed MSA unit cell. Dual-band absorption can be

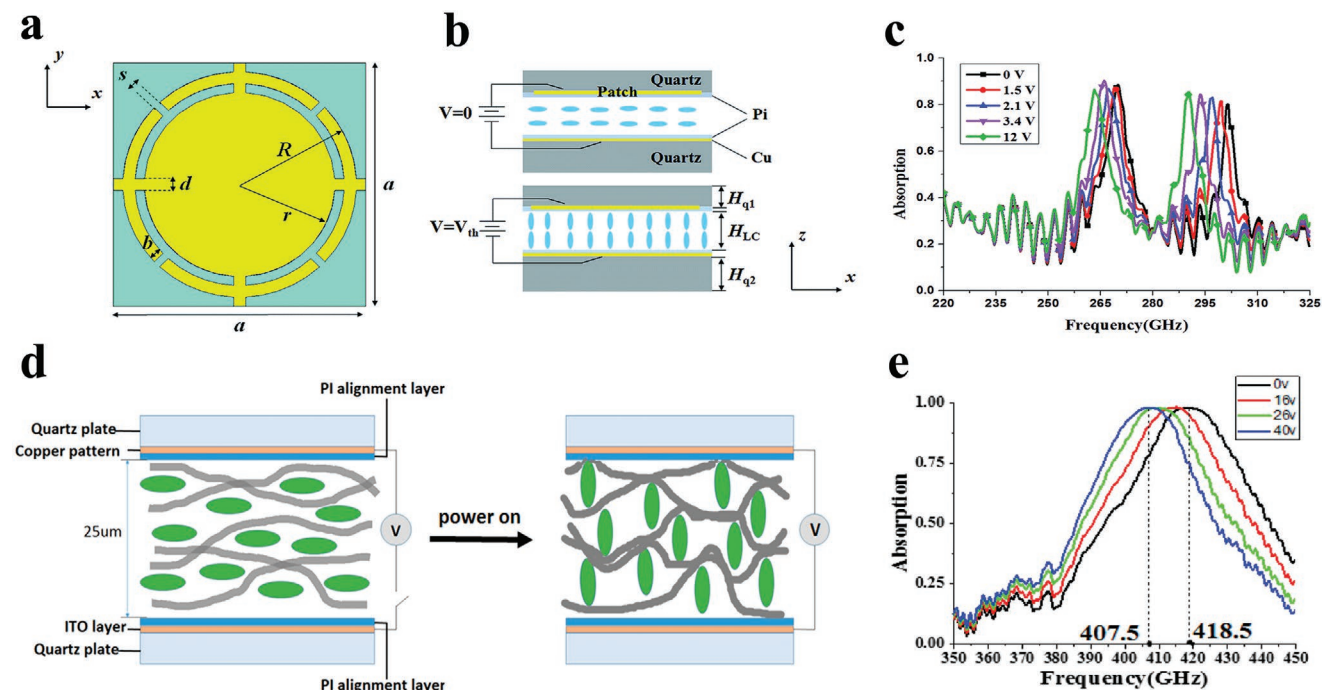


Figure 5. Tunable reconfigurable metasurface absorbers (MSAs) using liquid crystals (LCs): a) a schematic of a unit cell, b) cross-section, and c) the measured absorption with respect to the bias voltage under a normal-incidence transverse-electric polarized wave. The resonance frequencies for both modes exhibit red shifting with increasing bias voltage. Polymer network L-based MSAs: d) cross-section unpowered and powered and e) absorption spectra after 90 min UV exposure for different applied voltages. a–c) Reproduced with permission.^[88] Copyright 2018, The Royal Society of Chemistry. d,e) Reproduced with permission.^[89] Copyright 2018, MDPI.

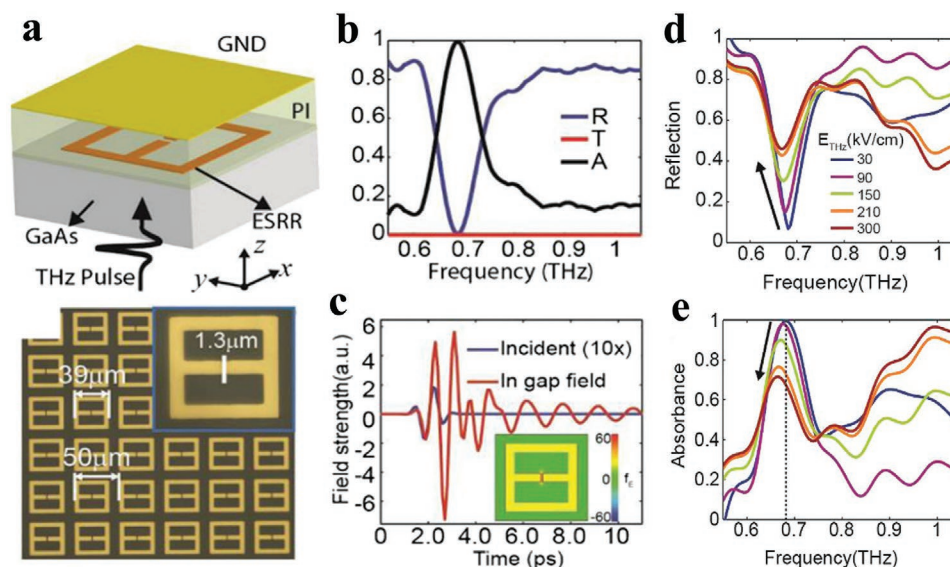


Figure 6. Optical reconfigurable metasurface absorbers (MSAs). MSAs on a GaAs substrate: a) a schematic and microscope image of the ESRR array (inset: close view of a unit cell); b) simulated transmission (T), reflection (R), and absorption (A) spectra; c) simulated time-domain field strength for the incident THz pulse (10 \times) and electric field in the middle of the capacitive gap (inset: 2D map of the electric field enhancement factor (f_e)); d) measured reflection spectra; and e) corresponding calculated nonlinear absorbance spectra for different THz field strengths. Reproduced with permission.^[47] Copyright 2016, Optical Society of America.

controlled electrically (2.45% and 3.65% for the first and second absorption peaks, respectively) by adjusting the LC bias voltage from 0–12 V, as shown in Figure 5c. Yin et al.^[89] also reported a fast-tunable sub-THz MSA based on a polymer network LC controlled by ultraviolet (UV) exposure and external bias voltage. Figure 5d,e shows the proposed structure, mechanism, and absorption spectra. The polymer network becomes more active after UV exposure and increasing the bias voltage continuously shifts the absorption peaks to lower frequencies until the LC molecules are fully rotated. Increasing the UV exposure time also causes a slight blue shift in peak absorption frequency for both the unbiased and fully biased states. Wang et al.^[48] suggested a tunable sub-THz MSA using graphene-assisted high-efficiency LCs for various applied voltages. The resulting MSA supported tunable resonance frequencies from 0.75 to 1 THz with a high-quality factor and $\approx 80\%$ amplitude modulation for the applied 10 V. A graphene layer provided a uniform static electric field to efficiently control the LCs under the influence of the externally supplied voltage.

3.2. Optical Tuning

Optical turning uses photoexcitation and THz pulses, and although complex biasing circuitry is unnecessary, a light- or power-sensitive material is required. For example, Huang and Cheng^[49] numerically demonstrated a tunable and polarization-insensitive photoexcitable MSA with wide-angle absorption in the sub-THz range. When the conductivity of the light-sensitive silicon (Si) chip combined with a copper film was changed from 1500 to 5×10^5 S m^{-1} using an incident laser, the absorption peak shifted from 0.615 to 0.321 THz. Cheng et al.^[90] used a photoconductive Si semiconductor to numerically investigate

a tunable MSA. The photoconductive semiconductor conductivity could be efficiently tuned using external THz pumping, resulting in a broadband switch with absorptions peaks from 0.82 to 0.51 THz and an absorption magnitude modulation depth of 62.2%. An active MSA based on the carrier dynamics in GaAs under an incident THz pulse was demonstrated theoretically and experimentally by Zhao et al.,^[47] as shown in Figure 6. The enhanced electric field caused carrier generation in the GaAs underneath the capacitive gaps of the electric splitting resonators. GaAs is a direct-band semiconductor material with a significant nonlinear response due to field-induced carrier dynamics. The authors measured a 20 GHz frequency shift and a 30% absorbance reduction when the incident field strength increased from 30 to 300 $kV\ cm^{-1}$, as shown in Figure 6d,e.

In this section, we discussed the absorption characteristics of active millimeter-wave and sub-THz MSAs. LCs and optical turning approaches are the main methods to control the MSA absorption frequency and ratio for these frequency bands. Applying these methods has led to changes in dielectric permittivity, surface impedance, and field interaction rather than controlling the resonators of microwave-region MSAs. Semiconductor diodes,^[91,92] MEMS, and other advanced tunable materials,^[93] such as (STO)^[94,95] and graphene,^[96] are also good candidates for active MSAs in these frequency bands. For example, Q et al.^[91] numerically investigated an MSA with tunable absorptivity from 65% to 99% using a semiconductor diode at 0.42 THz. Meanwhile, Hu et al.^[93] experimentally demonstrated a dynamically tunable sub-THz MSA based on an electrostatic MEMS actuator and an electrical dipole resonator array that achieved approximately 10% and 20% central resonance frequency and amplitude modulation, respectively, by applying different voltages. Winson et al.^[96] proposed a wide-band MSA

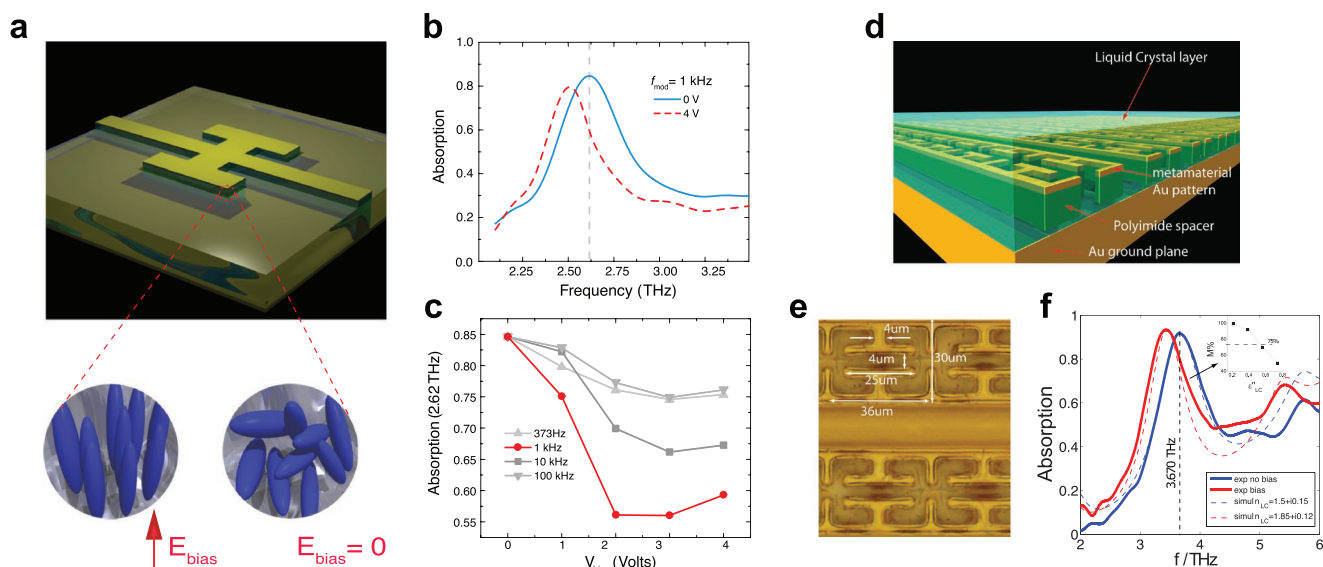


Figure 7. Liquid crystal (LC)-based electrically controlled reconfigurable metasurface absorbers (MSAs): a) a unit cell and measured results under different b) supply voltages and c) modulation frequencies (f_{mod}). An LC-based spatial light modulator (SLM) MSA for the THz region: d) 3D profile, e) photograph, and f) simulation and experimental results. a–c) Reproduced with permission.^[101] Copyright 2013, American Physical Society. d–f) Reproduced with permission.^[102] Copyright 2014, Wiley-VCH.

for the millimeter-wave range using graphene. The absorption was calculated based on the surface impedance, which was controlled by the chemical potential with support from Cu, SiO₂, and poly-Si layers. The advantages of MEMS and graphene for active MSAs are discussed in greater depth in the next section.

4. Reconfigurable MSAs for the THz, Optical, and Infrared Regions

Terahertz, infrared, and optical bands have attracted strong research interest due to their great potential in wireless communication, biomedicine, and security fields.^[97–99] In the previous sections, we presented several techniques for designing active MSAs for the microwave, millimeter-wave, and sub-THz regions whereas, in the current section, we discuss tunable/switchable MSAs for very high frequencies realized through employing advanced materials and fabrication technologies.

4.1. LCs

The previous section discussed how LCs can be used to realize frequency tunability in the millimeter-wave and sub-THz regions. LCs can also be used with very high frequencies, such as THz, optical, and infrared bands.^[100] Shrekenhamer et al.^[101] first demonstrated a tunable MSA based on electrically controlled LCs in 2013. LC permittivity was controlled by applying a square-wave potential between an ERR and the ground plane. **Figure 7b** shows that the resonance frequency shifted from 2.62 to approximately 2.5 THz by tuning the bias voltage from 0 to 4 V. The absorption magnitude can also be controlled by considering the modulation frequency (f_{mod}). Savo et al.^[102] reported an active MSA spatial light modulator (SLM) for the THz range.

The device was arranged into a 6×6 pixel matrix electrically controlled by an external bias voltage. Numerical simulations were confirmed experimentally, and the authors showed that the absorption peak at 3.67 THz (no bias) shifted to a lower frequency in the bias case (**Figure 7f**).

4.2. Graphene

Graphene-based electrical control has been used to achieve device reconfigurability for a very high frequency band. Graphene was discovered in 2004,^[103] and its conductance can be tuned by controlling the external electrostatic or magnetostatic fields.

Xiang et al.^[104] proposed a tunable dual-band absorber based on L-shaped graphene resonators. A thin layer of SiO₂ was used as a dielectric substrate between the top layer of the graphene pattern and the ground plane. **Figure 8b,c** shows that increasing the number of L-shaped elements from one to two in a unit cell increased the absorption peak from 50% to 98.77%. Two almost perfect absorption peaks occurred at 10.87 and 13.43 μm for 0.55 eV, with continuous tuning being obtained by controlling the Fermi energy of the graphene pattern. A tunable MSA based on a graphene–silver hybrid has been proposed for operation in the mid-infrared band.^[104] The top layer consisted of poly(ethylene oxide) and graphene on a SiO₂ dielectric spacer (see **Figure 8e,f**). Silver was employed as a ground plane on the bottom layer to capture the electromagnetic waves. Tuning was achieved from 4.25 to 5.75 μm by changing the chemical potential from 1 to 2 eV, corresponding to 76.4–100% absorptivity. On the other hand, a dual-band tunable metamaterial absorber has been achieved by designing different orientations of the elliptical shape graphene resonators on the surface, as shown in **Figure 8h**.^[105] By controlling the chemical potential from 0.3 to 0.5 eV, the absorption peaks

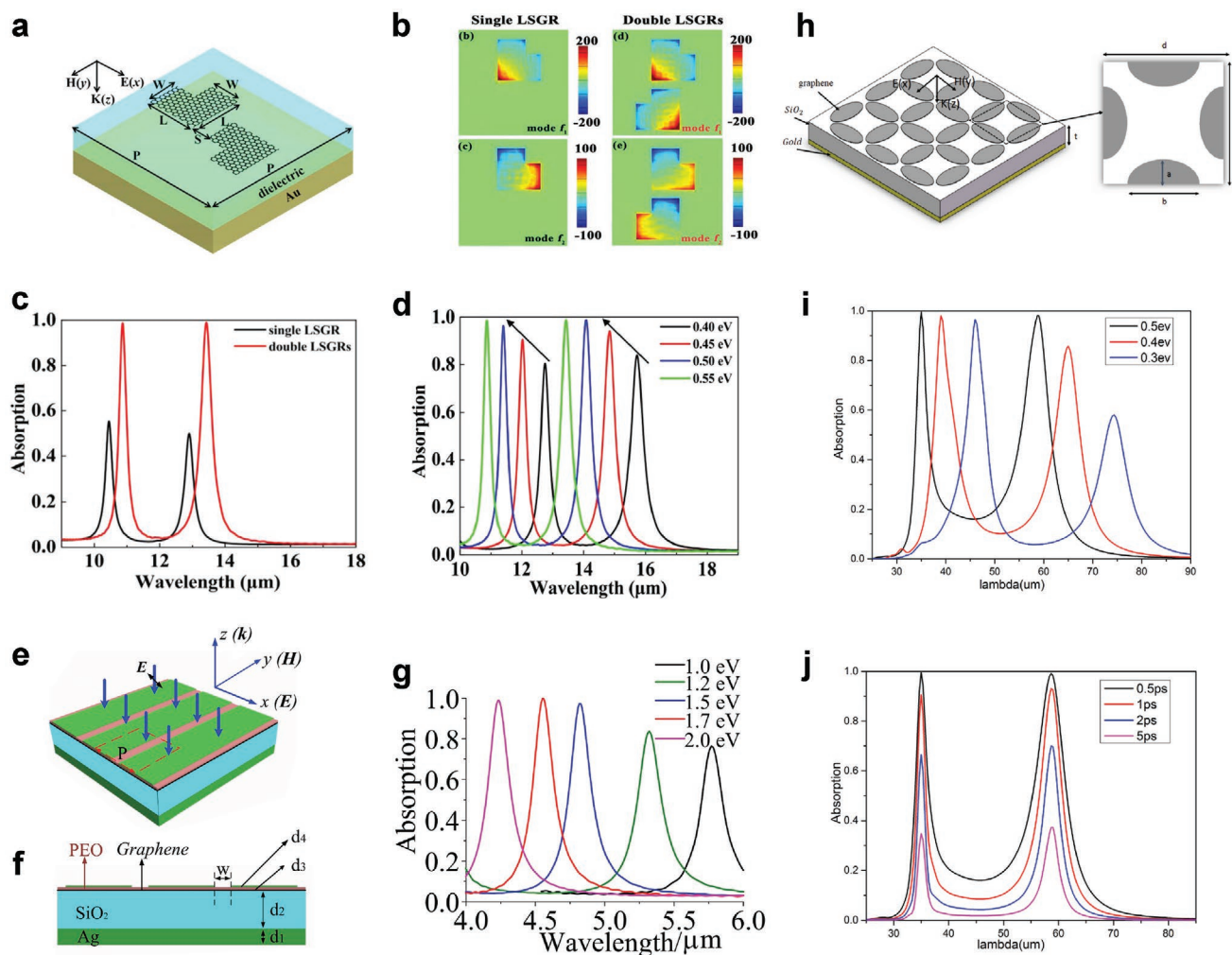


Figure 8. Graphene-based reconfigurable metasurface absorbers (MSAs): a) a unit cell and b) electric field distribution for single and dual L-shaped graphene resonators (LSGRs). Numerical simulations for c) single- and dual-band LSGRs, and d) tunable dual-band LSGRs. A graphene–silver hybrid MSA for the mid-infrared region: e) unit cell, f) structure, and g) simulation for different chemical potentials. h) Geometrical dimensions of a graphene-based elliptical absorber. Simulated results of the absorption spectra for different i) Fermi level and j) relaxation times. a–d) Reproduced with permission.^[104] Copyright 2019, IEEE. e–g) Reproduced with permission.^[113] Copyright 2018, IEEE. h–j) Reproduced with permission.^[105] Copyright 2016, Optical Society of America.

can be tuned from 35 to 46 μm and from 58 to 75 μm , with corresponding absorptivity values of 96–99.99% and 57–98%, as exhibited in Figure 8i. In addition, their absorption magnitudes can be adjusted by controlling the relaxation times (Figure 8j).

4.3. MEMS

Previous sections have discussed MSA tuning by modifying the dielectric substrate or conductance property. It is also possible to use MEMS to physically change the gap between the MM unit cells, the distance between the substrates, etc. For example, a tunable infrared MSA has been demonstrated based on electrostatic control.^[106] The structure consisted of four layers of Babinet MMs with the dielectric layer spaced by an air gap between the metallic ground plane and its supporting substrate. The top layer was pulled down onto the ground plane

(snap-down state) by applying a bias voltage and returned to the equilibrium position (snap-back state) when no bias was applied (see Figure 9a). In the snap-down state, the structure achieved high absorptivity at 6.2 μm wavelength with a measured reflection of 34.5%. Low absorptivity was obtained when the top layer returned to the equilibrium state (Figure 9c,d).

Liu et al.^[107] have recently demonstrated a high-performance tunable absorber based on a MEMS-driven MM for the THz frequency region. The top layer consisted of metallic meta-atoms on a silicon nitride membrane separated by an air gap from the ground plane. Figure 10 shows the measured absorption spectra of three devices (S1, S2, and D2) with different applied voltages. D2 was measured until snap-down (i.e., the bias voltage was increased above the snap-down threshold) whereas S1 and S2 were measured below the snap-down threshold. The resonance frequency shifted by 165 GHz ($\approx 206\%$ resonance linewidth) with a 65% change in absolute absorption.

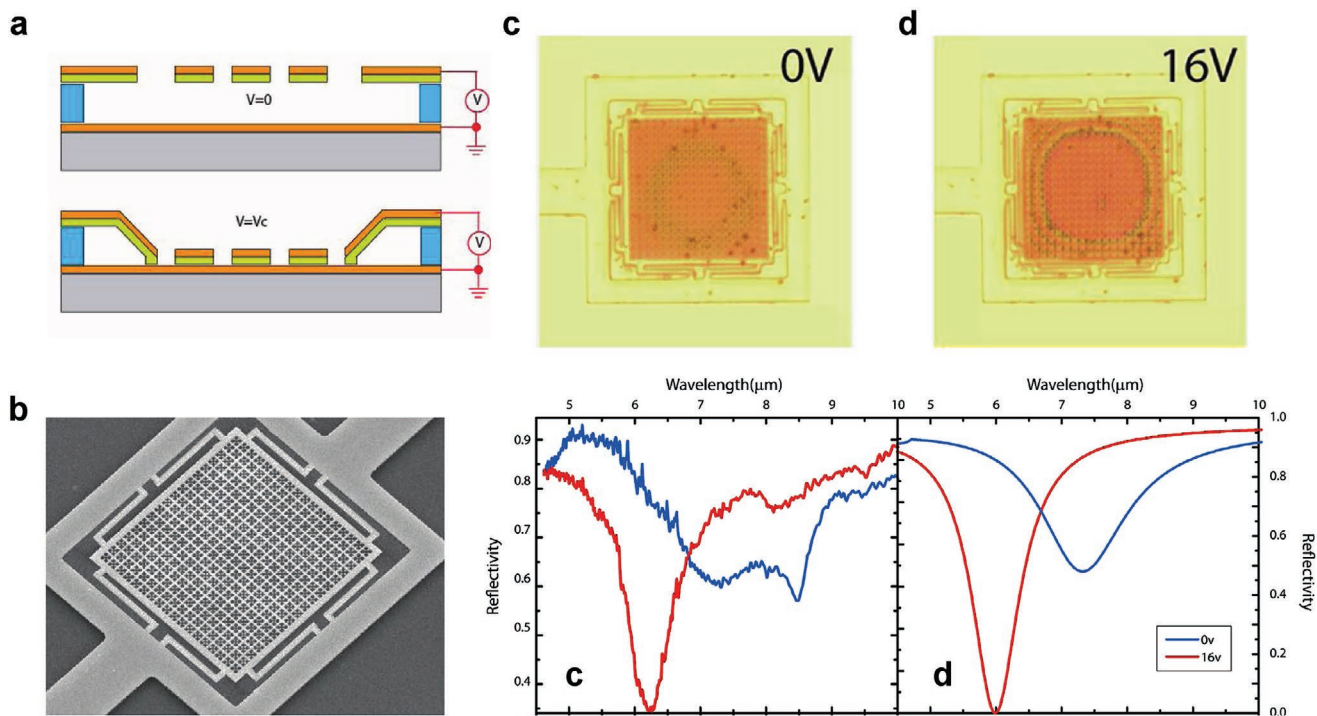


Figure 9. Tunable infrared metasurface absorbers (MSAs): a) snap-back and snap-down states, b) SME image and optical images at c) 0 V (snap-back) and d) 16 V (snap-down), and the e) measured and f) simulated reflectivity at 0 and 16 V. Reproduced with permission.^[106] Copyright 2014, Wiley-VCH.

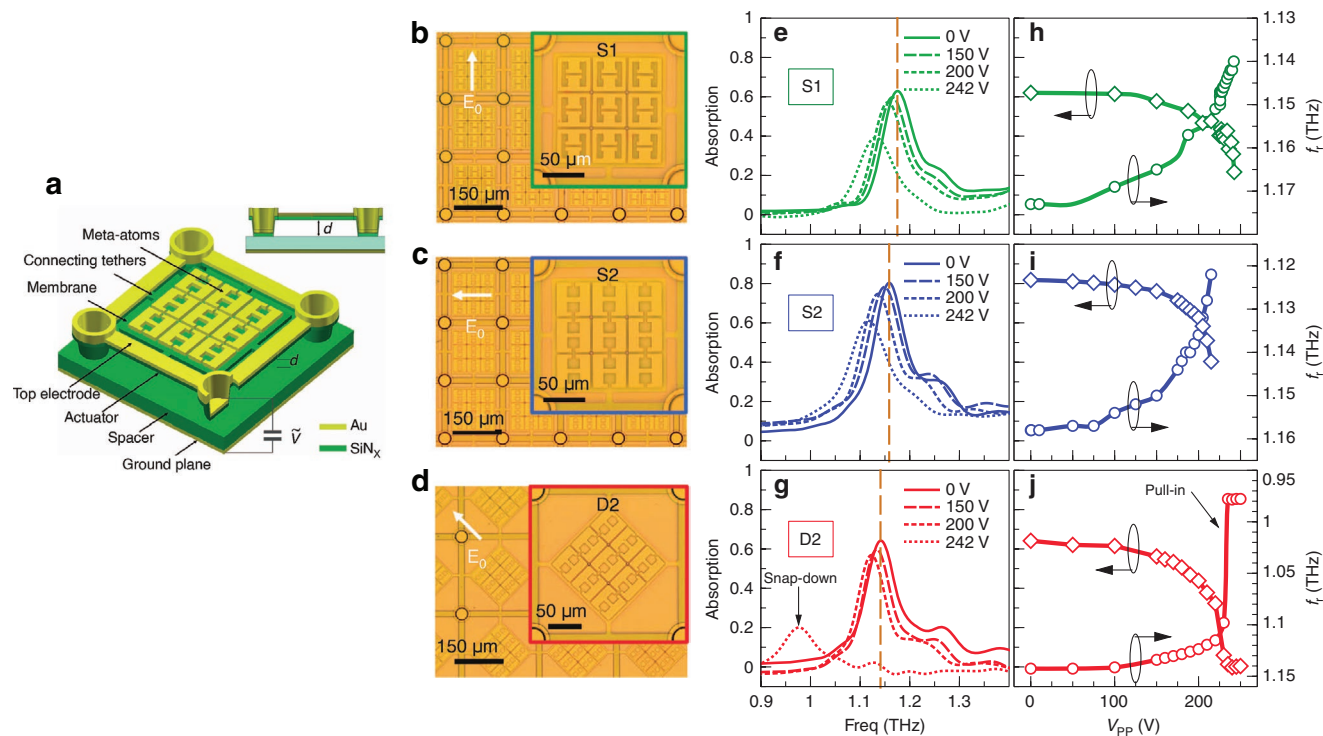


Figure 10. Microelectromechanical system (MEMS)-based metasurface absorbers (MSAs). a) Unit cell; b) S1, c) S2, and d) D2 device images; e–g) the measured absorption spectra at different applied voltages; and h–j) the measured absorption peaks and corresponding resonance frequencies with respect to the bias voltage for each of the respective devices. Reproduced with permission.^[107] Copyright 2017, Nature Publishing Group.

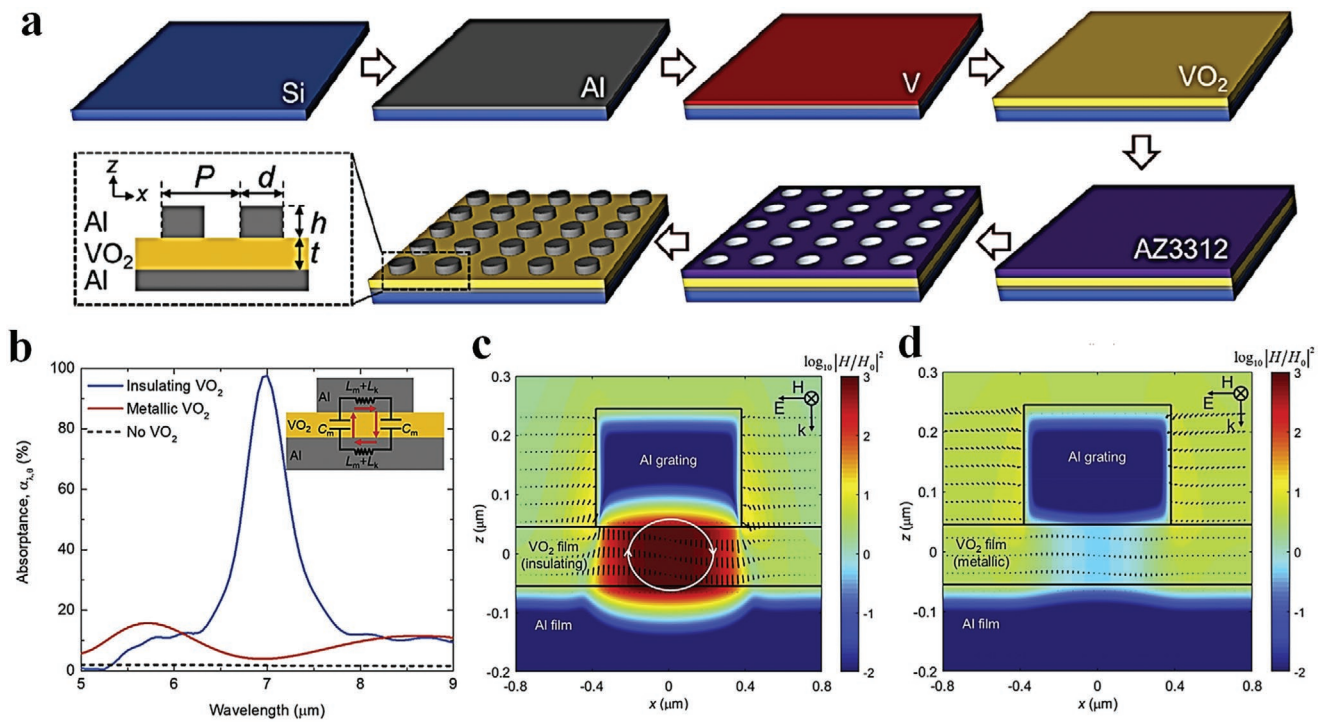


Figure 11. Vanadium dioxide (VO_2)-based reconfigurable metasurface absorbers (MSAs): a) the fabrication process, b) absorptivity in different states, and the electromagnetic field distributions in the c) amorphous and d) crystalline states. Reproduced with permission.^[109] Copyright 2019, Elsevier B.V.

4.4. Vanadium Dioxide (VO_2)

Phase-change materials' (PCMs) resistivity changes rapidly depending on the temperature. Active PCM-based MSAs have been recently investigated because they can switch phase states quickly.^[72,108,109]

Vanadium dioxide (VO_2) is a well-known material used in thermal PCMs for MSAs operating in the THz band.^[108–111] VO_2 can change phase states due to heating, which can be exploited in active MSAs. For example, Long et al.^[109] proposed a thermally switchable MSA/emitter using a VO_2 phase-change layer as a complete layer in the substrate. The VO_2 phase can be altered between amorphous (insulating) and crystalline (conductive) states either side of the transition temperature (68 °C). When VO_2 is in an amorphous state (e.g., at room temperature), capacitance occurs between the top metallic patterns and bottom metallic ground plane, as shown in Figure 11c, thereby producing resonance and absorptivity (Figure 11b). However, when VO_2 enters the crystalline state (above 68 °C) and thus becomes conductive, the top conductive patterns and the bottom ground plane are shorted. Therefore, there is no resonance or absorption response when VO_2 is in the crystalline state (Figure 11d).

5. Conclusions

In this paper, we reviewed the recent literature regarding reconfigurable MSAs using advanced materials. The latter comprise an important research topic to overcome MSAs' narrow bandwidth problems. We introduced advanced materials used in MSAs categorized by the latter's operation in the microwave,

millimeter and sub-THz, and THz regions. Figure 12 shows the frequency-tuning range of reconfigurable MSAs for each tuning material. In the microwave region, PIN diodes, DI water, and liquid metals can provide high-frequency tuning ratios (>100%), while STO, varactor diodes, and GeTe can realize low-frequency tuning ratios (<42%). In the millimeter and sub-THz regions, photoexcitable materials achieve the highest frequency-tuning ratio (62.8%), followed by LCs (28.5%) and THz pulse (2.98%). For the THz region, VO_2 achieves the highest frequency-tuning ratio (97%), whereas graphene, MEMS, and LCs achieve 30%,

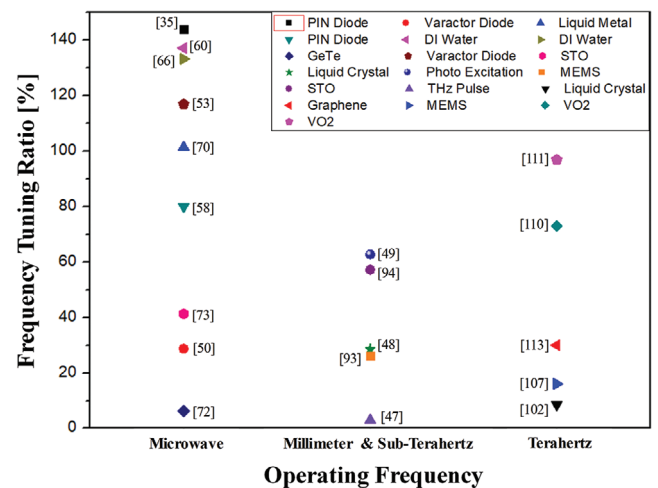


Figure 12. Performance comparison of reconfigurable metasurface absorbers (MSAs) using advanced materials. The reference for each advanced material is noted beside it in the figure.

Table 1. Current reconfigurable metasurface absorbers using advanced materials.

Refs.	Tuning material	Operating frequency band	Frequency tuning ratio ^{a)} [%]	Tuning method	Tuning speed ^{c)}	Maximum incident angle ^{b)} [°]	Polarization sensitivity	Fabrication ^{c)}	Cost ^{c)}	Tuning state
[35]	PIN diode	Microwave (1.7–10.46 GHz)	144	Electrical	Fast	N/A	Insensitive	Simple	Medium	Switching
[53]	Varactor diode	Microwave (0.98–3.78 GHz)	117	Electrical	Fast	N/A	Insensitive	Simple	Medium	Continuous
[70]	Liquid metal	Microwave (4–12.24 GHz)	101.4	Fluidic	Very slow	60	Insensitive	Simple	Medium	Switching
[60]	DI water	Microwave (5.58–30 GHz)	137.2	Fluidic	Very slow	45	Insensitive	Simple	Low	Continuous
[72]	GeTe	Microwave (9.6–10.23 GHz)	6.3	Thermal	Medium	No	Sensitive	Complex	High	Switching
[73]	STO	Microwave (0.48–0.73 GHz)	41.3	Thermal	Medium	70	Insensitive	Medium	Medium	Switching
[48]	Liquid crystal	Millimeter and sub-THz (750–1000 GHz)	28.5	Electrical	Fast	N/A	Sensitive	Complex	Medium	Continuous
[49]	Photoexcitation	Millimeter and sub-THz (321–615 GHz)	62.8	Optical	Medium	60	Insensitive	Complex	High	Continuous
[47]	THz pulse	Millimeter and sub-THz (660–680 GHz)	2.98	Electrical	Fast	N/A	Sensitive	Complex	High	Continuous
[93]	MEMS	Millimeter and sub-THz (550–720 GHz)	26.15	Mechanical	Slow	N/A	Sensitive	Complex	High	Continuous
[94]	STO	Millimeter and sub-THz (111–200 GHz)	57.23	Thermal	Medium	N/A	Insensitive	Medium	Medium	Continuous
[102]	Liquid crystal	THz (3.37–3.67 THz)	8.58	Electrical	Fast	N/A	Sensitive	Complex	Medium	Switching
[113]	Graphene	THz (4.25–5.75 μm)	30	Electrical	Fast	N/A	Sensitive	Complex	Medium	Continuous
[107]	MEMS	THz (1.14–1.175, 1.12–1.16, and 0.97–1.14 THz)	3.02, 3.5, 16.1	Mechanical	Slow	N/A	Sensitive	Complex	High	Continuous
[111]	VO ₂	THz (1.627–4.696 μm)	97	Thermal	Medium	N/A	Sensitive	Complex	High	Switching

^{a)}Frequency tuning ratio (%) = $(f_{\text{high}} - f_{\text{low}})/f_{\text{center}} \times 100$; ^{b)}Incidence angle to maintain higher than 90% absorptivity; ^{c)}estimated.

16.1%, and 8.58%, respectively. **Table 1** summarizes other performance parameters of the reconfigurable MSAs, such as maximum incident angle, polarization sensitivity, fabrication difficulty, cost, tuning speed, and tuning state. The maximum incident angle is defined as the angle at which higher than 90% absorptivity is attained. The fabrication complexity and cost are estimated from the proposed fabrication processes. Tuning technology can be categorized as electrical, optical, thermal, and fluidic. In the microwave region, various tuning methods can be used. The fluidic tuning method is simple and cheap to fabricate in spite of the slow tuning speed. Currently, liquid metal and fluidic materials are limited to the microwave region. On the other hand, the electrical tuning method shows the

fastest tuning speed, although the fabrication cost and complexity become higher as the frequency increases. Because of limited tuning materials, electrical tuning methods using LCs and graphene are widely used for the THz region. Optical tuning methods are generally used in the millimeter and sub-THz regions because they have medium tuning speed and fabrication complexity. Thermal tuning methods have the potential to be used for operation in the THz region because of the wider tuning range and moderate tuning speed. Varactor diodes, LCs, photoexcitation, THz pulse, MEMS, STO, and graphene can achieve the continuous tuning state whereas other tuning materials can only switch between two states. Reconfigurable MSAs with incidence angle and polarization insensitivity have

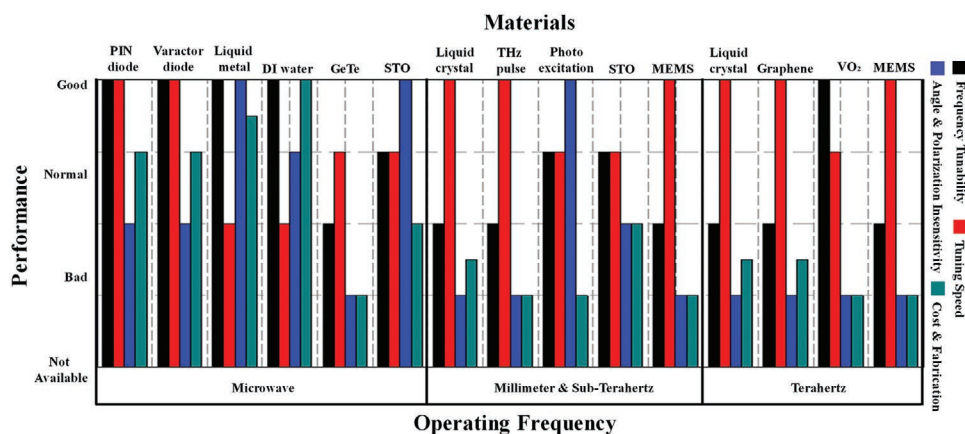


Figure 13. Performance comparison graph of reconfigurable metasurface absorber (MSA) materials to compare the advantages and disadvantages of each material.

been mostly studied for the microwave region. However, they need to be developed for the millimeter-wave and THz regions. Although most THz MSAs are sensitive to the polarization angle, polarization insensitivity can be easily achieved via symmetric unit cells. **Figure 13** shows a comparison graph to visualize the advantages and disadvantages of each approach. Therefore, we can determine suitable frequency-tuning materials depending on the target application. This review of these materials may enable the creation of new trends in active MSA research and analysis that will be very important in the future.

Acknowledgements

This work was supported by the National Research Foundation of Korea funded by the Korean Government (grant 2017R1A2B3003856).

Conflict of Interest

The authors declare no conflict of interest.

Keywords

frequency-selective absorbers, metamaterials, metasurfaces, reconfigurable metasurfaces

Received: December 27, 2019
Revised: February 25, 2020
Published online:

[1] D. R. Smith, J. B. Pendry, M. C. K. Wiltshire, *Science* **2004**, *305*, 788.
[2] S. X. Ta, I. Park, *IEEE Antennas Wireless Propag. Lett.* **2014**, *13*, 587.
[3] P. Prakash, M. P. Abegaonkar, A. Basu, S. K. Koul, *IEEE Antennas Wireless Propag. Lett.* **2013**, *12*, 1315.
[4] D. Kim, J. Yeo, *IEEE Antennas Wireless Propag. Lett.* **2008**, *7*, 718.
[5] K. Li, C. Zhu, L. Li, Y. M. Cai, C. H. Liang, *IEEE Antennas Wireless Propag. Lett.* **2013**, *12*, 678.
[6] B. P. Smyth, S. Barth, A. K. Iyer, *IEEE Trans. Antennas Propag.* **2016**, *64*, 5046.

[7] D. Cure, T. M. Weller, F. A. Miranda, *IEEE Trans. Antennas Propag.* **2013**, *61*, 506.
[8] L. Li, J. Wang, J. Wang, H. Du, H. Huang, J. Zhang, S. Qu, Z. Xu, *Appl. Phys. Lett.* **2015**, *106*, 212904.
[9] R. Phon, S. Ghosh, S. Lim, *IEEE Trans. Antennas Propag.* **2019**, *67*, 1709.
[10] T. J. Cui, M. Q. Qi, X. Wan, J. Zhao, Q. Cheng, *Light: Sci. Appl.* **2014**, *3*, e218.
[11] J. Ju, D. Kim, J. Lee, J. Choi, *Microwave Opt. Technol. Lett.* **2009**, *51*, 1973.
[12] H. Attia, L. Yousefi, M. M. Bait-Suwailam, M. S. Boybay, O. M. Ramahi, *IEEE Antennas Wireless Propag. Lett.* **2009**, *8*, 1198.
[13] C. M. Watts, X. Liu, W. J. Padilla, *Adv. Mater.* **2012**, *24*, 98.
[14] N. I. Landy, S. Sajuyigbe, J. J. Mock, D. R. Smith, W. J. Padilla, *Phys. Rev. Lett.* **2008**, *100*, 207402.
[15] H. Jeong, T. T. Nguyen, S. Lim, *Sci. Rep.* **2018**, *8*, 1.
[16] W. Wang, C. Xu, M. Yan, A. Wang, J. Wang, M. Feng, J. Wang, S. Qu, *IEEE Access* **2019**, *7*, 150969.
[17] L. He, L. Deng, Y. Li, H. Luo, J. He, S. Huang, S. Yan, *Appl. Phys. A: Mater. Sci. Process.* **2019**, *125*, 1.
[18] H. Lv, Z. Yang, H. Xu, L. Wang, R. Wu, *Adv. Funct. Mater.* **2020**, *30*, 1907251.
[19] A. Feng, M. Ma, Z. Jia, M. Zhang, G. Wu, *RSC Adv.* **2019**, *9*, 25932.
[20] Y. Li, Z. Liu, H. Zhang, P. Tang, B. Wu, G. Liu, *Opt. Express* **2019**, *27*, 11809.
[21] K. C. Opiela, T. G. Zielinski, *Composites, Part B* **2020**, *187*, 107833.
[22] L. J. Du Toit, *IEEE Antennas Propag. Mag.* **1994**, *36*, 17.
[23] J. B. Kim, J. H. Byun, *IEEE Trans. Electromagn. Compat.* **2012**, *54*, 37.
[24] C. Hu, L. Lin, P. Chen, C. Gong, W. Liu, *J. Phys. Commun.* **2019**, *3*, 045003.
[25] N. T. Q. Hoa, P. D. Tung, N. D. Dung, H. Nguyen, T. S. Tuan, *AIP Adv.* **2019**, *9*, 065318.
[26] T. T. Nguyen, S. Lim, *Sci. Rep.* **2018**, *8*, 6633.
[27] T. T. Nguyen, S. Lim, *Sci. Rep.* **2017**, *7*, 3204.
[28] R. Yahiaoui, S. Tan, L. Cong, R. Singh, F. Yan, W. Zhang, *J. Appl. Phys.* **2015**, *118*, 083103.
[29] A. Tittl, A. K. U. Michel, M. Schäferling, X. Yin, B. Gholipour, L. Cui, M. Wuttig, T. Taubner, F. Neubrech, H. Giessen, *Adv. Mater.* **2015**, *27*, 4597.
[30] N. I. Landy, C. M. Bingham, T. Tyler, N. Jokerst, D. R. Smith, W. J. Padilla, *Phys. Rev. B* **2009**, *79*, 125104.
[31] J. W. Park, P. Van Tuong, J. Y. Rhee, K. W. Kim, W. H. Jang, E. H. Choi, L. Y. Chen, Y. Lee, *Opt. Express* **2013**, *21*, 9691.
[32] X.-Y. Peng, B. Wang, S. Lai, D. H. Zhang, J.-H. Teng, *Opt. Express* **2012**, *20*, 27756.

- [33] S. Ghosh, S. Lim, *IEEE Antennas Wireless Propag. Lett.* **2018**, *17*, 2379.
- [34] H. Xiong, J. S. Hong, C. M. Luo, L. L. Zhong, *J. Appl. Phys.* **2013**, *114*, 064109.
- [35] H. Jeong, S. Lim, in *APS/URSI 2018: IEEE Int. Symp. on Antennas and Propagation and USNC-URSI Radio Science Meeting*, IEEE, Piscataway, NJ **2018**, p. 2325.
- [36] A. Y. Modi, C. A. Balanis, C. R. Birtcher, H. N. Shaman, *IEEE Trans. Antennas Propag.* **2019**, *67*, 298.
- [37] S. Liu, H. Chen, T. J. Cui, *Appl. Phys. Lett.* **2015**, *106*, 1.
- [38] L. H. Gao, Q. Cheng, J. Yang, S. J. Ma, J. Zhao, S. Liu, H. B. Chen, Q. He, W. X. Jiang, H. F. Ma, Q. Y. Wen, L. J. Liang, B. B. Jin, W. W. Liu, L. Zhou, J. Q. Yao, P. H. Wu, T. J. Cui, *Light: Sci. Appl.* **2015**, *4*, e324.
- [39] L. Ali, Q. Li, T. A. Khan, J. Yi, X. Chen, *Materials* **2019**, *12*, 1.
- [40] Y. Liu, S. Gu, C. Luo, X. Zhao, *Appl. Phys. A* **2012**, *108*, 19.
- [41] F. Ding, Y. Cui, X. Ge, Y. Jin, S. He, *Appl. Phys. Lett.* **2012**, *100*, 1.
- [42] J. Zhao, Q. Cheng, J. Chen, M. Q. Qi, W. X. Jiang, T. J. Cui, *New J. Phys.* **2013**, *15*, 043049.
- [43] N. Zhang, P. Zhou, D. Cheng, X. Weng, J. Xie, L. Deng, *Opt. Lett.* **2013**, *38*, 1125.
- [44] J. Mei, G. Ma, M. Yang, Z. Yang, W. Wen, P. Sheng, *Nat. Commun.* **2012**, *3*, 756.
- [45] L. Zigoneanu, B. I. Popa, A. F. Starr, S. A. Cummer, *J. Appl. Phys.* **2011**, *109*, 054906.
- [46] M. Badreddine Assouar, M. Senesi, M. Oudich, M. Ruzzene, Z. Hou, *Appl. Phys. Lett.* **2012**, *101*, 173505.
- [47] X. Zhao, J. Zhang, K. Fan, G. Duan, G. D. Metcalfe, M. Wraback, X. Zhang, R. D. Averitt, *Photonics Res.* **2016**, *4*, A16.
- [48] L. Wang, S. Ge, W. Hu, M. Nakajima, Y. Lu, *Opt. Express* **2017**, *25*, 23873.
- [49] M. Huang, Y. Cheng, in *2018 IEEE Int. Conf. on Computational Electromagnetics (ICCEM 2018)*, IEEE, Piscataway, NJ **2018**, pp. 1–3.
- [50] H. Yuan, B. O. Zhu, Y. Feng, *J. Appl. Phys.* **2015**, *117*, 173103.
- [51] V. A. Libi Mol, C. K. Anandan, in *2017 Progress in Electromagnetics Research Symp. – Fall (PIERS-FALL 2017)*, IEEE, Piscataway, NJ **2017**, pp. 1685–1689.
- [52] X. Wu, C. Hu, Y. Wang, M. Pu, C. Huang, C. Wang, X. Luo, *AIP Adv.* **2013**, *3*, 022114.
- [53] S. Ghosh, K. V. Srivastava, *IEEE Trans. Antennas Propag.* **2017**, *65*, 4903.
- [54] N. Hu, J. Zhang, S. Zha, C. Liu, H. Liu, P. Liu, *IEEE Antennas Wireless Propag. Lett.* **2019**, *18*, 373.
- [55] H. Jeong, S. Lim, *Sci. Rep.* **2018**, *8*, 1.
- [56] S. Ghosh, K. V. Srivastava, *IEEE Trans. Antennas Propag.* **2016**, *64*, 3665.
- [57] D. Lee, H. Jeong, S. Lim, *Sci. Rep.* **2017**, *7*, 1.
- [58] B. Zhu, C. Huang, Y. Feng, J. Zhao, T. Jiang, *Prog. Electromagn. Res. B* **2010**, *24*, 121.
- [59] Y. Zhou, Z. Shen, X. Huang, J. Wu, Y. Li, S. Huang, H. Yang, *Solid State Phys.* **2019**, *1*, 6.
- [60] J. R. A. J. Y. Yin, *Opt. Mater. Express* **2018**, *9*, 2060.
- [61] J. Xie, W. Zhu, I. D. Rukhlenko, F. Xiao, C. He, J. Geng, X. Liang, R. Jin, M. Premaratne, *Opt. Express* **2018**, *26*, 5052.
- [62] J. Xie, S. Quader, F. Xiao, C. He, X. Liang, J. Geng, R. Jin, W. Zhu, I. D. Rukhlenko, *IEEE Antennas Wireless Propag. Lett.* **2019**, *18*, 536.
- [63] Z. Wu, X. Chen, Z. Zhang, L. Heng, S. Wang, Y. Zou, *Appl. Phys. Express* **2019**, *12*, 057003.
- [64] Z. Shen, X. Huang, H. Yang, T. Xiang, C. Wang, Z. Yu, J. Wu, *J. Appl. Phys.* **2018**, *123*, 225106.
- [65] P. J. Bradley, M. O. M. Torrico, C. Brennan, Y. Hao, *Sci. Rep.* **2018**, *8*, 14490.
- [66] Y. Pang, Y. Shen, Y. Li, J. Wang, Z. Xu, S. Qu, *J. Appl. Phys.* **2018**, *123*, 155106.
- [67] H. Z. Zhao, Y. J. Zhou, in *2018 Cross Strait Quad-Regional Radio Science Wireless Technology Conf. (CSQRWC 2018)*, IEEE, Piscataway, NJ **2018**, pp. 1–3.
- [68] K. Ling, H. K. Kim, M. Yoo, S. Lim, *Sensors* **2015**, *15*, 28154.
- [69] H. K. Kim, D. Lee, S. Lim, *Sci. Rep.* **2016**, *6*, 31823.
- [70] S. Ghosh, S. Lim, *Sci. Rep.* **2018**, *8*, 1.
- [71] K. Ling, K. Kim, S. Lim, *Opt. Express* **2015**, *23*, 21375.
- [72] H. Jeong, J. H. Park, Y. H. Moon, C. W. Baek, S. Lim, *Sensors* **2018**, *18*, 3506.
- [73] L. Wang, D. Xia, Q. Fu, Y. Wang, X. Ding, B. Yang, *J. Electromagn. Waves Appl.* **2019**, *33*, 1406.
- [74] T. A. Khan, A. Alkhateeb, R. W. Heath, *IEEE Trans. Wireless Commun.* **2016**, *15*, 6048.
- [75] F. Topfer, J. Oberhammer, *IEEE Microwave Mag.* **2015**, *16*, 97.
- [76] C. Fiandrino, H. Assasa, P. Casari, J. Widmer, *Proc. IEEE* **2019**, *107*, 732.
- [77] M. Burla, C. Hoessbacher, W. Heni, C. Haffner, Y. Fedoryshyn, D. Werner, T. Watanabe, H. Massler, D. Elder, L. Dalton, J. Leuthold, *APL Photonics* **2019**, *4*, 056106.
- [78] M. Li, K. M. Luk, *IEEE Trans. Antennas Propag.* **2015**, *63*, 3276.
- [79] B. P. S. Sahoo, C. C. Chou, C. W. Weng, H. Y. Wei, *IEEE Consum. Electron. Mag.* **2019**, *8*, 49.
- [80] C. Zhang, J. Yang, W. Cao, W. Yuan, J. Ke, L. Yang, Q. Cheng, T. Cui, *Photonics Res.* **2019**, *7*, 478.
- [81] X. Zhang, Z. Hu, in *2013 European Microwave Conf.*, IEEE, Piscataway, NJ **2013**, pp. 1043–1046.
- [82] F. Yang, J. Gong, E. Yang, Y. Guan, X. He, S. Liu, X. Zhang, Y. Deng, *Appl. Phys. A: Mater. Sci. Process.* **2019**, *125*, 1.
- [83] S. Lai, Y. Wu, X. Zhu, W. Gu, W. Wu, *IEEE Photonics J.* **2017**, *9*, 1.
- [84] A. Vahidi, H. Rajabalipanah, A. Abdolali, A. Cheldavi, *Appl. Phys. A* **2018**, *124*, 337.
- [85] Y. Lu, B. Chi, D. Liu, S. Gao, P. Gao, Y. Huang, J. Yang, Z. Yin, G. Deng, *ACS Omega* **2018**, *3*, 11144.
- [86] K. Fan, W. J. Padilla, *Mater. Today* **2015**, *18*, 39.
- [87] C. C. Tartan, J. J. Sandford O'Neill, P. S. Salter, J. Aplinc, M. J. Booth, M. Ravnik, S. M. Morris, S. J. Elston, *Adv. Opt. Mater.* **2018**, *6*, 1800515.
- [88] Z. Yin, Y. Lu, T. Xia, W. Lai, J. Yang, H. Lu, G. Deng, *RSC Adv.* **2018**, *8*, 4197.
- [89] Z. Yin, C. Wan, G. Deng, A. Zheng, P. Wang, Y. Yang, S. Gao, J. Yang, F. Cai, Z. Li, H. Lu, *Appl. Sci.* **2018**, *8*, 2454.
- [90] Y. Cheng, R. Gong, Z. Cheng, *Opt. Commun.* **2016**, *361*, 41.
- [91] Q. Li, Z. Tian, X. Zhang, R. Singh, L. Du, J. Gu, J. Han, W. Zhang, *Nat. Commun.* **2015**, *6*, 7082.
- [92] L. Qi, C. Li, G. Fang, *Int. J. Electromagn. Appl.* **2014**, *4*, 57.
- [93] F. Hu, N. Xu, W. Wang, Y. Wang, W. Zhang, J. Han, W. Zhang, *J. Micromech. Microeng.* **2016**, *26*, 025006.
- [94] B.-X. Wang, X. Zhai, G.-Z. Wang, W.-Q. Huang, L.-L. Wang, *Opt. Mater. Express* **2015**, *5*, 227.
- [95] B. X. Wang, G. Z. Wang, *J. Mater. Sci.: Mater. Electron.* **2017**, *28*, 8487.
- [96] D. Winson, B. Choudhury, N. S. Kumar, H. Barshilia, R. U. Nair, *IEEE Trans. Antennas Propag.* **2019**, *67*, 1.
- [97] C. Sirtori, *Nature* **2002**, *417*, 132.
- [98] M. Tonouchi, *Nat. Photonics* **2007**, *1*, 97.
- [99] T. W. Crowe, *IEEE Trans. Microwave Theory Tech.* **2003**, *50*, 910.
- [100] G. Isić, B. Vasić, D. C. Zografopoulos, R. Beccherelli, R. Gajić, *Phys. Rev. Appl.* **2015**, *3*, 064007.
- [101] D. Shrekenhamer, W. C. Chen, W. J. Padilla, *Phys. Rev. Lett.* **2013**, *110*, 177403.
- [102] S. Savo, D. Shrekenhamer, W. J. Padilla, *Adv. Opt. Mater.* **2014**, *2*, 275.
- [103] K. S. Novoselov, A. K. Geim, S. V. Morozov, D. Jiang, Y. Zhang, S. V. Dubonos, I. V. Grigorieva, A. A. Firsov, *Science* **2004**, *306*, 666.
- [104] Y. Xiang, L. Wang, Q. Lin, S. Xia, M. Qin, X. Zhai, *IEEE Photonics Technol. Lett.* **2019**, *31*, 483.
- [105] G. Yao, F. Ling, J. Yue, C. Luo, J. Ji, J. Yao, *Opt. Express* **2016**, *24*, 1518.
- [106] X. Liu, W. J. Padilla, *Adv. Opt. Mater.* **2013**, *1*, 559.

- [107] M. Liu, M. Susli, D. Silva, G. Putrino, H. Kala, S. Fan, M. Cole, L. Faraone, V. P. Wallace, W. J. Padilla, D. A. Powell, M. Martyniuk, I. V. Shadrivov, *Microsyst. Nanoeng.* **2017**, *3*, 17033.
- [108] R. Sun, P. Zhou, W. Ai, Y. Liu, Y. Li, R. Jiang, W. Li, X. Weng, L. Bi, L. Deng, *Opt. Express* **2019**, *27*, 11537.
- [109] L. Long, S. Taylor, X. Ying, L. Wang, *Mater. Today Energy* **2019**, *13*, 214.
- [110] H. Liu, Z. H. Wang, L. Li, Y. X. Fan, Z. Y. Tao, *Sci. Rep.* **2019**, *9*, 1.
- [111] L. Lei, F. Lou, K. Tao, H. Huang, X. Cheng, P. Xu, *Photonics Res.* **2019**, *7*, 734.
- [112] S. Ghosh, K. V. Srivastava, *IEEE Antennas Wireless Propag. Lett.* **2017**, *16*, 1687.
- [113] S. Cao, T. Wang, Q. Sun, Y. Tang, B. Hu, U. Levy, W. Yu, *IEEE Photonics Technol. Lett.* **2018**, *30*, 475.